# Regeneration dynamics of iron and nutrients from bay sediment into bottom water of Funka Bay, Japan

Nanako Hioki, Kenshi Kuma*, Yuichiroh Morita, Daichi Miura, Atsushi Ooki, Seiji Tanaka, Hiroji Onishi, Tetsuya Takatsu, Naoto Kobayashi, Yoshihiko Kamei

Faculty of Fisheries Sciences, Hokkaido University, 3-1-1 Minato, Hakodate, Hokkaido 041-8611, Japan

*Corresponding author: Kenshi Kuma, Faculty of Fisheries Sciences, Hokkaido University, 3-1-1 Minato, Hakodate, Hokkaido 041-8611, Japan
Tel & Fax: +81-138-40-8823; E-mail: kuma@fish.hokudai.ac.jp

Short Title: Iron in a subarctic coastal environment

Key words: Iron cycling, Nutrients, Dissolved oxygen, Humic-like dissolved organic matter, Bay sediment, Funka Bay (Japan).

## Abstract

We studied iron remobilization and nutrient regeneration in bottom water of Funka Bay, Japan, bimonthly from August 2010 to December 2011. The bay basin (bottom depth, 92–96 m) is separated from the northwest Pacific Ocean at its mouth by a sill with a depth of 60 m. After a spring phytoplankton bloom during early March–early April, nutrients in bay bottom water tended to accumulate with time until August–September and to increase gradually with depth during April–October by the oxidative decomposition of settling particulate organic matter on the bay bottom. In contrast, the process of iron remobilization into bottom water of the bay is remarkably different from nutrient regeneration. The much higher concentrations of dissolved and total dissolvable iron near the bottom and the seasonally variable relationship between dissolved iron concentration and apparent oxygen utilization in bay bottom water likely reflect a balance between dissolved iron input and removal processes within the bay bottom water. The release of soluble Fe(II) from reducing bay sediments might induce the high concentrations of dissolved and total dissolvable iron in deep–bottom waters of Funka Bay and might be one of the most important sources of iron in Funka Bay. The upward transport of iron from the bay bottom to the surface water during the winter vertical mixing may play an important role on the supply of bioavailable iron for phytoplankton growth in the coastal waters.

## 1. Introduction

Iron is one of the most important micronutrients for phytoplankton growth in the ocean. Despite the great interest in the behavior of iron in open oceans, our understanding of the biogeochemical and physical mechanisms that regulate iron as well as nutrients is still limited in coastal regions. The concentration of dissolved iron (D-Fe) in remote oceanic regions is characteristically low relative to concentrations in coastal environments in close proximity to terrestrial and continental shelf sources of iron. The iron distributions in coastal waters are more dynamic and complicated than in oceanic environments, being subject to varying influences of atmospheric input, run-off from continents, shelf sediments, vertical and horizontal mixing, and phytoplankton productivity. Many recent studies highlight the potential importance of sedimentary iron sources for the coastal ocean, and even the open ocean (e.g., Lam et al. 2006; Hurst et al. 2010; Severmann et al. 2010). The release of Fe(II) from reducing continental shelf sediments might be one of the most important sources of iron in coastal waters (Lohan and Bruland 2008; Homoky et al. 2012a, b). Enrichment of iron in pore fluids and bottom waters is driven by the reductive dissolution of insoluble Fe(III) during the decomposition of organic matter.

Funka Bay, Japan, has an area of 2300 $km^2$ with maximum depth of 96 m, and is separated from the northwestern North Pacific Ocean at its only entrance by a sill with 60-m depth (Figure 1). The seasonal changes in hydrographic conditions in Funka Bay have been reported in detail by several previous studies (e.g. Ohtani and Akiba 1970; Ohtani 1971; Ohtani and Kido 1980). Water exchange in this bay occurs periodically twice a year, with Oyashio water (OW) in early spring and Tsugaru warm water (TW) in early autumn (Ohtani 1971). In most years, there is a massive spring phytoplankton bloom in this bay, consisting mainly of chain-forming diatoms *Thalassiosira* spp. and *Chaetoceros* spp., for approximately ten days during early

March–early April (e.g. Maita and Odate 1988; Kudo and Matsunaga 1999; Shinada et al. 1999; Kudo et al. 2000, 2007; Yoshimura and Kudo 2011). One-third of the annual primary production in Funka Bay occurs during the spring bloom (Kudo and Matsunaga 1999). After the spring bloom, there is extensive settling and sedimentation of particulate organic matter on the bay bottom (Miyake et al. 1998), and the bottom water tends to be isolated from the surface during summer (Takahashi et al. 2005; Kudo et al. 2007).

In this study, we measured the seasonal vertical distributions of iron, nutrients, dissolved oxygen, and humic-like fluorescent dissolved organic matter (FDOM, measured as humic-like fluorescence intensity [humic F-intensity]) in the water column of three stations in the deepest part of Funka Bay located close together in the center of the bay. Humic F-intensity as well as water properties (temperature, salinity, and density) is very useful to discriminate between OW and TW (Saitoh et al. 2008; Kuma et al. 2014). In particular, our goal was to determine the factors controlling the seasonal distributions of iron in comparison with those of nutrients in bottom water of Funka Bay considering the sediment–water interface and water exchange after the spring bloom and to show the potential importance of sedimentary iron sources in the semi-closed benthic layer of Funka Bay for phytoplankton growth in the coastal waters.

## 2. Materials and methods

### 2.1 Sample collection and treatment

Sampling was conducted from the R/V *Ushio-Maru* at three stations, closely located in the center of the Funka Bay basin: Stn 23 (42°24.0′N, 140°31.0′E, bottom depth 95 m), Stn 30 (42°16.2′N, 140°36.0′E, bottom depth 92 m), and Stn 33 (42°19.0′N, 140°30.5′E,

bottom depth 96 m) (Fig.1). Water samples were collected bimonthly during August 2010–February 2011 for all three stations and then during April–December 2011 for Stn 30. Samples were collected from water depths of 5 to 86 m at Stn 30 and from 5 to 90 m at Stn 23 and Stn 33 using acid-cleaned, Teflon®-coated, 5-L Niskin X sampling bottles (General Oceanics) attached to a rosette multi-sampler along with a conductivity-temperature-depth (CTD) probe (SBE 19plus, Sea-Bird Electronics, Inc.).

Samples for analysis of D-Fe, nutrients, and humic F-intensity were gravity filtered on deck by connecting an acid-cleaned 0.22-μm pore-size membrane filter (Millipak 100, Durapore cartridge type, Millipore) to a sampling spigot on the Niskin X bottles. The filtered samples (7−8 mL) in 10-mL acrylic tubes for nutrient and humic F-intensity analyses were immediately frozen and kept below –20 °C in the dark until measurements in the laboratory. Unfiltered samples were collected for total dissolvable iron (T-Fe) and dissolved oxygen (DO) concentrations. The filtered (<0.22-μm fraction) and unfiltered seawater samples (100 mL) used for D-Fe and T-Fe analyses, respectively, were initially collected in pre-cleaned, 125-mL low density polyethylene bottles, which were then acidified with ultrapure grade HCl to pH 1.7–1.8 in a Class 100 clean room in the laboratory on shore and then allowed to stand at room temperature for three months until analyzed for iron in the laboratory (Bruland and Rue 2001). Sample treatment in the present study is the same as in our previous studies (e.g., Uchida et al. 2013). Hydrographic observations (salinity, temperature, and depth) were conducted with a CTD attached to the sampling rosette. Additional water samples for determining nutrients and DO concentrations in bottom water were collected approximately 0.5–1 m above the bottom at each station using a Van Dorn sampling bottle on a steel wire. In addition, a DO sensor (RINKO I, Alec Electronics Co. Ltd., Japan) was deployed at approximately 90-m depth at Stn 30 to continuously measure the DO concentration in bottom water from April to October 2010 and 2011. The DO sensor was calibrated with the oxygen-saturated seawater by bubbling air after

bimonthly pulling up on deck and then was deployed again.

2.2 Dissolved and total dissolvable iron

Acidified iron samples were buffered at pH 3.2 with a buffer solution of 8.15 M quartz-distilled formic acid and 4.54 M ultrapure grade ammonium hydroxide (0.8 mL per 100 mL sample solution) in a class 100 clean room in the laboratory onshore. The iron concentrations (D-Fe and T-Fe) in buffered 0.22-μm-filtered and unfiltered samples were determined by an automated iron analyzer (Kimoto Electric Co. Ltd., Japan) using a combination of chelating-resin concentration and luminol–hydrogen peroxide chemiluminescence (CL) detection in a closed flow-through system (Obata et al. 1993) as described in our previous studies (e.g., Kitayama et al. 2009). Briefly, iron in a buffered sample was selectively collected on 8-hydroxyquinoline immobilized chelating resin and then eluted with dilute (0.3 M) HCl. The eluent was mixed successively with luminol solution, 0.6 M aqueous ammonia, and 0.7 M $H_2O_2$, and then the mixture was introduced into the CL cell. Finally, the iron concentration was determined from the CL intensity. The accuracy of this analysis was checked using SAFe (Sampling and Analysis of Fe) reference materials (pH 1.7–1.8). The D-Fe in the SAFe surface (S) water and deep (D1) intercalibration waters, as determined by our analytical method in the present study after being buffered at pH 3.2, were 0.10 ± 0.01 nM ($n$ = 6) for S and 0.70 ± 0.03 nM ($n$ = 5) for D1, consistent with the community consensus values of 0.090 ± 0.007 nM for S and 0.67 ± 0.07 nM for D1 (Johnson 2007; GEOTRACES [www.geotraces.org]).

2.3 Nutrients, dissolved oxygen, and humic-like FDOM

Concentrations of major nutrients ($NO_3$ + $NO_2$, $PO_4$, and $Si(OH)_4$) were determined by

using an autoanalyzer (Technicon) using CSK standard solutions for nitrate and nitrite (Wako Pure Chemical Industries, Ltd., Japan) and standard methods (Parsons et al. 1984). Dissolved oxygen was determined onboard by the Winkler titration method with potentiometric end-point using a 798 MPT Titrino analyzer (Metrohm). Apparent oxygen utilization (AOU) was calculated by subtracting the measured oxygen content from the dissolved oxygen concentration at saturation under in situ temperature and salinity (Hansen 1999).

Humic-like FDOM was quantified by measuring humic F-intensity, as reported in our previous studies (e.g., Uchida et al. 2013). The frozen 0.22-µm-filtered samples in acrylic tubes were thawed and warmed overnight to room temperature in the dark, and then the humic F-intensity was measured in a 1-cm quartz cell by using a fluorescence spectrophotometer (model F-2000, Hitachi) at 320 nm excitation and 420 nm emission wavelengths and 10-nm bandwidths (Hayase et al. 1988; Hayase and Shinozuka 1995). It has been reported that the storage in acrylic tube under freezing conditions does not measurably affect the humic F-intensity of seawater samples (e.g., Uchida et al. 2013; Tanaka et al. 2014). Fluorescent intensity is expressed in terms of quinine sulfate units (1 QSU = 1 ppb quinine sulfate in 0.05 M $H_2SO_4$, excitation 320 nm, emission 420 nm; Mopper and Schultz [1993]).

## 3 Results

### 3.1 Hydrographic features

Water properties (in-situ temperature [$T$], salinity [$S$], and density [$\sigma_T$]) were similar throughout the water column at all three stations during August 2010–February 2011. Therefore, we show the vertical profiles of water properties (Fig. 2) and the

191 temperature–salinity diagram (Fig. 3) only for Stn 30 during August 2010–December
192 2011. The salinities of typical OW and TW are below 33.3 and above 33.7, respectively
193 (Ohtani 1971; Ohtani and Kido 1980, Fig. 3). Salinities in the upper 30 m of the water
194 column in August 2010 and 2011 and in June 2011 were low (<32.5; Figs. 2, 3a, b) due
195 to the surface inflow of OW and the inflow of meltwater after April (Hasegawa and
196 Isoda 1997). After August, the surface salinity increased rapidly from early autumn to
197 early winter as a result of the inflow of TW. Typical Funka Bay winter water (FW) with
198 consistently low temperature and high salinity ($T < 6$ °C, $S > 33.3$; Fig. 3) is formed by
199 vertical mixing during winter after the intrusion of TW in autumn and early winter
200 (Ohtani and Akiba 1970; Ohtani and Kido 1980). Values for *T, S,* and $\sigma_T$ in February
201 and December 2011 (Figs. 2, 3) were almost unvaryingly constant throughout the water
202 column, with narrow ranges for *T* and *S* ($T$ = 4–5 °C, $S$ = 33.4–33.6 in February 2011
203 and $T$ = 9 °C, $S$ = 33.6–33.8 in December 2011). After February, surface salinity
204 decreased gradually from April to August as a result of OW inflow, although FW
205 remained as bottom water during spring and summer (Fig. 3c, d). There was a stronger
206 intrusion of TW into the bottom water during August, October, and December in 2011
207 than in 2010 (Fig. 3c, d).
208
209 3.2 Humic F-intensity, nutrients, and dissolved oxygen
210
211 During August 2010–February 2011, relatively similar distributions of humic
212 F-intensity and nutrients and DO concentrations were observed throughout the water
213 column at all three stations, although nutrient and DO concentrations in deep-bottom
214 waters, except for near bottom, in October 2010 are different between the stations
215 (lower nutrient and higher DO concentrations at Stn 33 and Stn 30 than Stn 23, data not
216 shown). We therefore show only the vertical profiles at Stn 30 during August
217 2010–February 2011 (Fig. 4a–e) and April–December 2011 (Fig. 4f–j). Below the

surface mixed layer, humic F-intensity in August 2010 was relatively uniform throughout the water column at all three stations, with higher values (2.0–2.7 QSU) than those during October 2010–February 2011 (Fig. 4a). From August to October 2010 the humic F-intensity in the upper 20–40 m decreased rapidly to about 1.5 QSU, and values in December 2010 and February 2011 were low (1.5 to 1.7 QSU) and vertically uniform throughout the water column at all stations. The humic F-intensity tended to increase with time from February to April–August 2011 and then to decrease with time from August to December, with a vertically uniform profile in December 2011, remarkably similar to profiles in December 2010 and February 2011 at all stations (Fig. 4a, f). However, low values (below 2 QSU) were observed at depths of 60–80 m at Stn 30 in August 2011 (Fig. 4f), very different from those in August 2010 (Fig. 4a).

During August–October 2010 and April–October 2011, $NO_3 + NO_2$ and $Si(OH)_4$ were depleted in the surface water (<20–40 m depth), whereas there was still measurable $PO_4$ in the surface water. All nutrient concentrations tended to increase with depth in waters below 30–40 m depth in April–October, with maxima in bottom water in August (Fig. 4b–d, g–i). Nutrient concentrations in February and December 2011, however, were remarkably uniform, with relatively high concentrations throughout the water column.

Dissolved oxygen concentrations in August, October, and December 2010 and 2011 at all three stations were 5–7 ml $L^{-1}$ in the upper 60 m and 1.5–5 ml $L^{-1}$ in the deep to bottom waters (60 m–near bottom; Fig. 4e, j). Dissolved oxygen concentrations below 2 ml $L^{-1}$ were found only in the bottom water (>80-m depth), with concentrations decreasing with depth at all stations in August 2010 (Fig. 4e), whereas no such low-DO bottom water was observed in August 2011 (Fig. 4j). Dissolved oxygen concentrations in February 2011 were remarkably uniform, with high concentrations of around 7 ml $L^{-1}$ throughout the water column at all stations. The highest DO concentrations (about 8 ml $L^{-1}$) were observed in the upper 40 m in April 2011. Dissolved oxygen

concentrations in the bottom water of Stn 30, which were measured at a depth of approximately 90 m (2 m above the bottom) by a DO sensor, showed seasonal variations from April to October (Fig. 5). In 2010, there was a continuous, rapid decrease in concentrations from 6–7 ml $L^{-1}$ in the middle of June to 1.5 ml $L^{-1}$ in late August–early September, followed by a rapid increase with a few sudden positive fluctuations from early September to October. In 2011, there was a gradual decrease from 5 ml $L^{-1}$ in April to 1.7 ml $L^{-1}$ in late August–early September, with several large positive fluctuations. The higher DO concentration in the bottom water on 18 August 2011 (4–5 ml $L^{-1}$, Fig. 4j) as compared to that on 23 August 2010 (<2 ml $L^{-1}$, Fig. 4e) is consistent with a large positive fluctuation in DO concentrations during 10–18 August 2011 (Fig. 5) although there were difference (approximately ±0.2 ml $L^{-1}$ at 1.5 ml $L^{-1}$ level and ±1 ml $L^{-1}$ at 5 ml $L^{-1}$ level) between DO concentrations determined by Winkler titration method and a DO sensor probably because of different sampling and deploying depths.

### 3.3 Dissolved and total dissolvable iron

Concentrations of D-Fe during August 2010–February 2011 had relatively similar vertical and seasonal distributions at all three stations (Fig. 6a–c). However, it was found that D-Fe levels and vertical profiles in bottom waters in October 2010 were different between the stations. In October 2010, D-Fe concentrations in bottom water at Stn 23 increased with depth to 10 nM (Fig. 6a), while those at Stn 33 and 30 were remarkably uniform with low concentrations of 1–2 nM throughout the water column (Fig. 6b–c). During August–December 2010 and April–October 2011, D-Fe concentrations were relatively low (around 1–5 nM) from the surface to depths of 50–60 m and tended to increase rapidly with depth in waters below 70 m to the maximum values (15–22 nM) in bottom water (around 90 m) in August 2010. However,

concentrations during winter 2011 increased gradually with depth from 4–7 nM at 5-m depth to 14–18 nM at around 90-m depth at all three stations in February 2011 (Fig. 6a–c), and from 5 nM in surface water to 9 nM in bottom water at Stn 30 in December 2011 (Fig. 6d).

T-Fe concentrations during August 2010–February 2011 also showed relatively similar vertical distributions at all three stations (Fig. 6e–g). In October 2010, however, T-Fe concentrations in bottom water at Stn 23 increased with depth to 400 nM (Fig. 6e), while those at Stn 33 and 30 were relatively uniform with low concentrations of about 50 nM (Fig. 6f, g). In the surface 20–40 m, T-Fe concentrations in August and October 2010 and 2011 and April 2011 were relatively low (around 4–27 nM). During winter, however, T-Fe concentrations were relatively high (around 28–60 nM) in December 2010 and February 2011, and in December 2011 they were vertically uniform and remarkably high (about 220–300 nM) in the upper 60 m of the water column (Fig. 6h). T-Fe concentrations in waters below 60 m tended to increase rapidly with depth to the maximum values (500–900 nM) in bottom water (around 90 m) in August 2010 and October 2011, and gradually with depth to approximately 180–250 nM during December 2010–August 2011.

## 4 Discussion

### 4.1 Water properties in Funka Bay

Temperature–salinity diagrams (Fig. 3) show the strong intrusion of TW into the deep–bottom waters in August 2011 and the strong presence of TW throughout the water column in October and December 2011 (Fig. 3d). However, there is no evidence of such extensive water exchange with TW in the water column in August–December

299 2010 (Fig. 3c). In addition, the remarkably constant *T, S,* and $\sigma_T$ values throughout the
300 water column in February and December 2011 (Figs. 2, 3) are due to the strong vertical
301 water mixing during winter.
302 Previous studies (Saitoh et al. 2008; Kuma et al. 2014) have found that humic
303 F-intensity is relatively low in TW (1–1.5 QSU), which originates from Japan Sea
304 surface water, and relatively high in OW (≥2 QSU), which originates from Okhotsk Sea
305 water. In the present study, the lower, vertically homogeneous humic F-intensities
306 (around 1.5–1.6 QSU) in February and December are consistent with the constant and
307 relatively high *S* and $\sigma_T$ values throughout the water column during winter, resulting
308 from vertical water mixing and predominance of water with TW origins (Figs. 2, 3, 4a,
309 f). After winter, the decrease in *S* and the increase in humic F-intensity to around 2–2.5
310 QSU from February to April–August are due to water exchange with OW with higher
311 humic F-intensity than TW. A plot of humic F-intensity against *S* below 70-m depth
312 showed that the bottom water in August and October 2010 was OW, whereas in
313 December 2010 and 2011 and in February 2011 it was TW (Fig. 7). However, the lower
314 humic F-intensity values in deep–bottom waters in August and October 2011 compared
315 to 2010 were due to the temporary intrusion of TW with lower humic F-intensity into
316 the deep–bottom waters in 2011 (Figs. 3c, d, 4a, f, 7).
317
318 4.2 Consumption of oxygen and nutrient regeneration in deep–bottom waters
319
320 In the surface water (<20–40 m depth during August–October 2010 and April–October
321 2011) after a spring phytoplankton bloom during early March–early April, $NO_3 + NO_2$
322 was depleted regardless of the $PO_4$ and $Si(OH)_4$ levels due to the consumption of $NO_3 +$
323 $NO_2$ by the phytoplankton (Fig. 4b–d, g–i). Kudo et al. (2000) reported that $NO_3$
324 depletion terminates the spring bloom in Funka Bay and $Si(OH)_4$ is further consumed
325 after the exhaustion of $NO_3$.

In general, DO concentrations in the deep–bottom waters below 60-m depth tend to decrease vertically toward summer, reaching seasonal minimum values in bottom water in August–September (Figs. 4e, j, 5). The decrease in DO concentrations in deep–bottom waters results from the consumption of oxygen by the microbial decomposition of settled particulate organic matter on the sediment surface layer after a spring bloom. However, DO concentrations then tend to increase toward fall–winter from the intrusion of TW (Kudo et al. 2007). Dissolved oxygen concentrations (Fig. 4e, j) as well as water properties (*T, S*; Fig. 2) and chemical components (humic F-intensity and nutrients; Figs. 4a–d, f–i) were vertically homogeneous during winter (December–February) because of the vertical mixing during winter. In the present study, DO concentrations below 2 ml $L^{-1}$ were observed in the bottom water below 80-m depth at all stations in August 2010, although similarly low concentrations were not observed in August 2011 (Fig. 4e, j). Inagaki et al. (2012, 2014) reported that the hypoxic (DO <2 ml $L^{-1}$) conditions in bottom water of Funka Bay influenced macrobenthos abundance and the growth of flathead flounder *Hippoglossoides dubius,* which is the dominant demersal fish species and an important fishery resource in Funka Bay. Higher DO concentrations (>2 ml $L^{-1}$) in August 2011 than in 2010 were due to the temporarily strong intrusion of TW with higher DO concentrations into the bottom water during 10–18 August 2011 (Figs. 4j, 5). We found that the TW intrusion also contributed strongly to temporarily lowering humic F-intensity and nutrient concentration in deep–bottom waters (Figs. 4–5).

All nutrient concentrations in bottom water tended to increase with time during April–August and then decrease with time during August–December (Fig. 4b–d, g–i). In bottom water (80–87 m) in 2011, however, $PO_4$ concentrations in June were the highest, while $NO_3$+$NO_2$ concentrations in June were the lowest and $Si(OH)_4$ concentrations in June were lower than those in August and/or October (Fig. 4g–i). Watanabe and Tsunogai (1984) found a remarkable maximum concentration of

353 interstitial $PO_4$ at the depth of about 10 cm (Stn 30) in spring and summer. This
354 probably results from desorption of $PO_4$ on sediment particles under anoxic condition
355 through the oxidative decomposition of settled particulate organic matter on the bay
356 bottom after the spring bloom. Therefore, the highest concentrations of $PO_4$ in June
357 among the season (Fig. 4h) may be due to the large upward flux of $PO_4$ from pore water
358 of sediment to bottom water. The upward flux of $PO_4$ from pore water may contribute
359 some extent to the increase in $PO_4$ in the bottom water during spring and summer. In
360 addition, Kudo et al. (2007) found that $NO_3 + NO_2$ in bottom water at Stn 30 did not
361 increase from April to June because of the remineralization to $NH_4$ from April to June.
362 Therefore, low $NO_3$+$NO_2$ in bottom water in April–June (Fig. 4g) is attributable to the
363 remineralization to $NH_4$ during April–June although we did not measure $NH_4$
364 concentrations in this study. Nutrient regeneration in Funka Bay bottom water was
365 accompanied by oxygen consumption. The ratio of $PO_4$ to AOU below 70-m depth,
366 which was determined from the slope of $PO_4$ vs AOU by a linear regression (Fig. 8a),
367 was ~0.0060. The ratio was nearly the same as a global mean value of $P:O_2$ regeneration
368 ratio (~0.0067, DeVries and Deutsch 2014). The *y*-intercept of a plot of $PO_4$
369 concentration vs. AOU was approximately ~0.95 μM $PO_4$, indicating preformed $PO_4$
370 with conservative properties. Kudo et al. (2007) reported that the different preformed
371 $PO_4$ value in each year was due to the different yearly $PO_4$ concentration after the
372 winter vertical mixing, which replenishes oxygen to the whole water column. In
373 contrast, the relatively linear relationship between $Si(OH)_4$ and AOU in bottom water
374 (Fig. 8b) probably results from the seasonally constant concentration of interstitial
375 $Si(OH)_4$ and flux of $Si(OH)_4$ at the sediment–water interface (Watanabe and Tsunogai
376 1984).
377 The relationship between $NO_3 + NO_2$ and AOU in bottom water was
378 seasonally scattered (Fig. 9a). In addition, the $(NO_3 + NO_2):PO_4$ ratios in August 2010
379 at all stations (≥85 m), in October 2010 at Stn 23 and Stn 30 (≥80 m), in April and June

2011 at Stn 30 (≥70 m), and in August 2011 at Stn 30 (~91 m) were 10.44±0.60, 7.52±0.10, 4.65±1.05 (±1SD), and 8.50 respectively (Fig. 9b). The ratios were significantly lower ($p$ <0.01, $t$-test) than the Redfield ratio of 16:1 during biological production and regeneration of organic matter. Kudo et al. (2007) also reported that dissolved inorganic nitrogen (DIN: $NO_3 + NO_2 + NH_4$) in bottom water at Stn 30 increased linearly with AOU, although $NO_3 + NO_2$ did not increase from April to June because of the remineralization to $NH_4$ from April to June and the oxidation of $NH_4$ to $NO_3$ in July. Therefore, the $(NO_3 + NO_2):PO_4$ ratios far below 16:1 in April and June 2011 at Stn 30 (Fig. 9b) are probably attributable to the high concentration of $NH_4$ in the bottom water during April–June (Kudo et al. 2007). However, the low $(NO_3 + NO_2):PO_4$ ratios (Fig. 9b) in deep–bottom waters (≥80–90 m) with low DO concentrations (around 2–3 ml $L^{-1}$ or less; Fig. 4e, j) at all stations in August 2010 and at Stn 23 and Stn 30 in October 2010 may be due to the denitrification/anammox that occurs in shelf bottom sediments. Denitrifying bacteria consume $NO_3$ instead of oxygen for respiration in low-oxygen pore waters, which causes a $NO_3$ deficiency relative to $PO_4$. In addition, anammox (anaerobic oxidation of ammonium using nitrite to nitrogen gas) is also an important sedimentary process. Similar observations have been made near the continental shelves of the Bering Sea, Chukchi Sea, Okhotsk Sea, and elsewhere (Yoshikawa et al. 2006; Chang and Devol 2009; Mordy et al. 2010; Horak et al. 2013; Hioki et al. 2014). Under oxygen-depleted conditions, denitrification and anammox processes occur in the water column. In this study, minimum DO concentrations in the water were found to be about 1 ml $L^{-1}$ (45 μM) where denitrification and anammox processes might be inhibited. Previous studies had reported the oxygen sensitivities to $N_2$ loss processes, where denitrification is only active at 2–4 μM DO (Devol 1978) and anammox was completely inhibited at higher than about 13.5 μM of DO (Jensen et al. 2008). It is likely that the denitrification and anammox occurred under more oxygen-depleted condition, like within the sediments.

407

408 4.3 Iron remobilization in bay deep–bottom waters

409

410 In the surface water (<20–40 m depth during August–October 2010 and April–October
411 2011) after a spring bloom, D-Fe and T-Fe concentrations are relatively high (around
412 1–5 nM for D-Fe and 4–27 nM for T-Fe, Fig. 6), as compared to the iron levels in
413 oceanic surface water (e.g., Kitayama et al. 2009; Uchida et al. 2013). The high iron is
414 probably attributable to high iron inputs from rivers, atmosphere, and shelf sediments
415 into nutrient-depleted surface water.

416 Recently, many studies have focused on benthic iron remobilization from
417 shelf sediments (e.g., Lohan and Bruland 2008; Moore and Braucher 2008; Severmann
418 et al. 2010; Homoky et al. 2012a, b). The increases in D-Fe and T-Fe concentrations
419 with depth in waters below 70 m (Fig. 6a–c, e–g) in August 2010 were largely
420 consistent with the increase in nutrient concentrations (Fig. 4b–d) and the decrease in
421 DO concentration (Fig. 4e) with depth in deep–bottom waters. However, we found that
422 the increases in D-Fe and T-Fe concentrations with depth near the bottom to remarkably
423 high concentrations in bottom water were rapid, as compared to the gradual increase in
424 nutrient concentrations and the gradual decrease in DO concentration with depth. The
425 sudden increase in D-Fe and T-Fe concentrations with depth in deep–bottom waters in
426 August 2010 probably resulted from a marked increase in soluble Fe(II) concentrations
427 in anaerobic pore waters near the bay sediment-water interface in addition to the release
428 of the dissolved Fe from biogenic particles, which would be related with DO and
429 nutrient concentrations. In previous study, the oxidation-reduction potential (Eh) values
430 in the sub-surface layer (around 5 cm) of the sediment at Stn 30 of the Funka Bay were
431 from 0 to –50 mV in February and decreased to around –200 mV in April (Sasaki et al.
432 2001). Under the low Eh values in the sub-surface layer, it is possible that the
433 denitrification ($CH_2O$ (organic carbon)+$NO_3^- \Rightarrow N_2+CO_2$) and the reduction to

434 water-soluble $Fe^{2+}$ ($CH_2O$+particulate $Fe(OH)_3 \Rightarrow Fe^{2+}+CO_2$) occur in the anaerobic bay
435 sediment through microbial utilization of oxygen from oxygen-containing compounds
436 such as nitrate and particulate Fe(III) hydroxide, respectively (Stigliani 1988).
437 Hypoxic and suboxic conditions in bottom water lead to an increased flux of
438 reduced Fe(II) from non-biogenic Fe (lithogenic particulate Fe) in the shelf sediments
439 because the oxidation rate of Fe(II) is slowed in a cold, low-oxygen environment
440 (Lohan and Bruland 2008; Homoky et al. 2012a, b). In the overlying cold bottom water,
441 the reduced Fe(II) then oxidizes to the less-soluble Fe(III), which may lead
442 subsequently to the formation of colloidal and particulate Fe(III) hydroxide and then to
443 the removal of colloidal and particulate Fe(III) from the water by aggregation and
444 particle scavenging (Kuma et al. 1996; Kitayama et al. 2009; Hioki et al. 2014).
445 Therefore, D-Fe concentrations in deep–bottom waters of Funka Bay are inferred to
446 reflect a balance between input and removal processes. The D-Fe removal process in
447 deep–bottom waters results in the rapid increase in D-Fe concentration with depth in
448 bottom water (Fig. 6a–c) and seasonally variable relationships between D-Fe
449 concentrations and AOU (Fig. 10), remarkably different from those between nutrients
450 and AOU (Figs. 8, 9a). Nutrients tend to accumulate conservatively in deep–bottom
451 waters predominantly by the oxidative decomposition of settling particulate organic
452 matter and the dissolution of biogenic silica on the bay bottom after the spring bloom.
453 The lower D-Fe and T-Fe concentrations near the bottom in August 2011 than
454 in August 2010 (Fig. 6) are due to the temporary intrusion of TW with low iron
455 concentrations into the deep–bottom waters in August 2011 (Figs. 3, 5). In addition, the
456 uniformly lower iron concentrations in deep–bottom waters in October 2010 at Stn 33
457 and Stn 30 than Stn 23 (Fig. 6a–c, e–g) are probably due to the temporary water renewal
458 by the intrusion into the deep-bottom waters at Stn 33 and Stn 30. Similar phenomena in
459 deep-bottom waters, except for near bottom, in October 2010 at the three stations were
460 observed for nutrient and DO (lower nutrient and higher DO concentrations at Stn 33

and Stn 30 than Stn 23, data not shown). The temporary water renewal in deep-bottom waters is an important mechanism for the reduction of iron and nutrients and the recovery of DO in deep-bottom waters of Funka Bay basin.

The wider depth ranges in the water column with homogenously high iron and nutrient concentrations in February and December 2011 compared to in December 2010 (Figs. 4, 6) are due to the stronger vertical water mixing from December to February (also evident in the remarkably constant *T, S,* and $\sigma_T$ values throughout the water column; Fig. 2). The vertical water mixing during winter in Funka Bay is the most important mechanism for transporting iron from the bay bottom to the surface water. The upward transport of iron during winter may play an important role on the supply of bioavailable iron for phytoplankton growth in the coastal waters.

The actual concentration of soluble iron in seawater is likely maintained primarily by complexation of D-Fe with organic, iron-binding ligands such as humic dissolved organic matter, which controls the solubility of Fe(III) hydroxide in seawater (Kuma et al. 1996; Chen et al. 2004; Kitayama et al. 2009). However, the D-Fe concentrations throughout the water column in February and December 2011 (approximately 5–18 nM; Fig. 6a–d) were extremely high relative to Fe(III) hydroxide solubility (approximately 0.3–0.4 nM), which was estimated by using an equation derived in our previous study for the relationship between Fe(III) hydroxide solubility and humic F-intensity in the central North Pacific Ocean (Kitayama et al. 2009): Fe(III) hydroxide solubility (nM) = 0.226 × humic F-intensity (QSU) – 0.045 ($R$ = 0.78, $n$ = 14) . Therefore, the extreme excess of D-Fe throughout the water column in February and December 2011 (Fig. 6a-d) is probably due to the presence of colloidal iron (both colloidal Fe(III) hydroxide and iron bound to colloidal organic matter) in the D-Fe fraction (<0.22-μm pore-size), resuspended from the bay sediment during the winter vertical mixing.

**Acknowledgments** We thank K. Toya for technical assistance. We also thank the captain and crew of the R/V *Ushio-Maru* of Hokkaido University for their help in sampling. We are grateful to two reviewers for their constructive and helpful comments on this work. This study was supported partly by a grant for 2010–2011 FYs Research Projects from the Hokusui Society Foundation, Sapporo, and a grant for Scientific Research (no. 22510001) from the Ministry of Education, Culture, Sports, Science and Technology, Japan

## References

Bruland KW, Rue EL (2001) Analytical methods for the determination of concentrations and speciation of iron. In: Turner DR, Hunter KA (eds) The biogeochemistry of iron in seawater. Wiley, Chichester, pp 255–289

Chang BX, Devol AH (2009) Seasonal and spatial patterns of sedimentary denitrification rates in the Chukchi Sea. Deep-Sea Res II 56: 1339–1350

Chen M, Wang W-X, Guo L (2004) Phase partitioning and solubility of iron in natural seawater controlled by dissolved organic matter. Global Biogeochem Cycles 18: GB4013, doi:10.1029/2003GB002160.

Devol AH (1978) Bacterial oxygen uptake kinetics as related to biological processes in oxygen deficient zones of the oceans. Deep-Se Res 25: 137–146

DeVries T, Deutsch C (2014) Large-scale variations in the stoichiometry of marine organic matter respiration. Nature Geosci 7: 890–894

Hansen HP (1999) Determination of oxygen In: Grasshoff K, Kremling K, Ehrhard M (eds) The Methods of seawater analysis. Wiley, New York, pp 75–89

Hasegawa N, Isoda Y (1997) Fresh water budget of Funka Bay. Umi to Sora, 73, 113–121 (in Japanese with English abstract)

516 Hayase K, Shinozuka N (1995) Vertical distribution of fluorescent organic matter along
517 with AOU and nutrients in the equatorial Central Pacific. Mar Chem 48: 283–290
518 Hayase K, Tsubota H, Sunada I, Goda S, Yamazaki H (1988) Vertical distribution of
519 fluorescent organic matter in the North Pacific. Mar Chem 25: 373–381
520 Hioki N, Kuma K, Morita Y, Sasayama R, Ooki A, Kondo Y, Obata H, Nishioka J,
521 Yamashita Y, Nishino S, Kikuchi T, Aoyama M (2014) Laterally spreading iron,
522 humic-like dissolved organic matter and nutrients in cold, dense subsurface water of
523 the Arctic Ocean. Sci Rep 4: 6775, doi:10.1038/srep06775
524 Homoky WB, Severmann S, McManus J, Berelson WM, Riedel TE, Statham PJ, Mills
525 RA (2012a) Dissolved oxygen and suspended particles regulate the benthic flux of
526 iron from continental margins. Mar Chem 134: 59–70
527 Homoky WB, Severmann S, Mills RA, Statham PJ, Fones GR (2012b) Pore-fluid Fe
528 isotopes reflect the extent of benthic Fe redox recycling: evidence from continental
529 shelf and deep-sea sediments. Geol 37: 751–754
530 Horak REA, Whitney H, Shull DH, C. W. Mordy CW, Devol AH (2013) The role of
531 sediments on the Bering Sea shelf N cycle: Insights from measurements of benthic
532 denitrification and benthic DIN fluxes. Deep-Sea Res II 94: 95–105
533 Hurst MP, Aguilar-Islas AM, Bruland KW (2010) Iron in the southeastern Bering Sea:
534 Elevated leachable particulate Fe in shelf bottom waters as an important source for
535 surface waters. Cont Shelf Res 30: 467–480.
536 Inagaki Y, Takatsu T, Ashida Y, Takahashi T (2012) Annual changes in macrobenthos
537 abundance in Funka Bay, Japan. Fish Sci 78: 647–659
538 Inagaki Y, Takatsu T, Kimura M, Kano Y, Takahashi T, Kamei Y, Kobayashi N, Maeda
539 T (2014) Improved growth of flathead flounder Hippoglossoides dubius in hypoxic
540 waters in Funka Bay, Japan. Fish Sci 80: 725–734
541 Jensen MM, Kuypers MMM, Lavik G, Thamdrup B (2008) Rates and regulation of
542 anaerobic ammonium oxidation and denitrification in the Black Sea. Limnol

Oceanogr 53: 23–36

Johnson KS (2007) Developing standards for dissolved iron in seawater. EOS Trans, AGU 88(11): 131–132

Kitayama S, Kuma K, Manabe E, Sugie K, Takata H, Isoda Y, Toya K, Saitoh S, Takagi S, Kamei Y, Sakaoka K (2009) Controls on iron distributions in the deep water column of the North Pacific Ocean: Iron(III) hydroxide solubility and marine humic-type dissolved organic matter. J Geophys Res 114: C08019, doi:10.1029/2008JC004754

Kudo I, Matsunaga K (1999) Environmental Factors affecting the occurrence and production of the spring phytoplankton bloom in Funka Bay, Japan. J Oceanogr 55: 505–513

Kudo I, Yoshimura T, Yanada M, Matsunaga K (2000) Exhaustion of nitrate terminates a phytoplankton bloom in Funka Bay, Japan: change in $SiO_4$:$NO_3$ consumption rate during the bloom. Mar Ecol Prog Ser 193: 45–51

Kudo I, Yoshimura T, Lee C–W, Yanada M, Maita Y (2007) Nutrient regeneration at bottom after a massive spring bloom in a subarctic coastal environment, Funka Bay, Japan. J Oceanogr 63: 791–801

Kuma K, Nishioka J, Matsunaga K (1996) Controls on iron(III) hydroxide solubility in seawater: the influence of pH and natural organic chelators. Limnol Oceanogr 41: 396–407

Kuma K, Sasayama R, Hioki N., Morita Y, Isoda Y, Hirawake T, Imai K, Aramaki T, Nakamura T, Nishioka J, Ebuchi N (2014) Chemical evidence for the origin of the cold water belt along the northeastern coast of Hokkido. J Oceanogr 70: 377–387

Lam PJ, Bishop JKB, Henning CC, Marcus MA, Waychunas GA, Fung IY (2006) Wintertime phytoplankton bloom in the subarctic Pacific supported by continental margin iron. Global Biogeochem Cycles 20: GB1006, doi:10.1029/2005GB002557

Lohan MC, Bruland KW (2008) Elevated Fe(II) and dissolved Fe in hypoxic shelf waters off Oregon and Washington: an enhanced source of iron to coastal upwelling regimes. Environ Sci Technol 42: 6462–6468

Maita Y, Odate T (1988) Seasonal changes in size-fractionated primary production and nutrient concentrations in the temperate neritic water of Funka Bay, Japan. J

574 Oceanogr Soc Japan 44: 268–279
575 Miyake H, Yanada M, Nishi T, Hoshizawa K (1998) Short-time variation in low trophic
576 level productivity and hydrographic conditions in Funka Bay. Mem Fac Fish Sci
577 Hokkaido Univ 45: 36–41
578 Mordy CW, Eisner LB, Proctor P, Stabeno P. Devol AH, Shull DH, Napp JM,
579 Whitledge T (2010) Temporary uncoupling of the marine nitrogen cycle:
580 Accumulation of nitrite on the Bering Sea Shelf. Mar Chem 121: 157–166
581 Moore JK, Braucher O (2008) Sedimentary and mineral dust sources of dissolved iron
582 in the world ocean. Biogeosciences 5: 631–656
583 Mopper K, Schultz CA (1993) Fluorescence as a possible tool for studying the nature
584 and water column distribution of DOC components. Mar Chem 41: 229–238
585 Obata H, Karatani H, Nakayama E (1993) Automated determination of iron in seawater
586 by chelating resin concentration and chemiluminescence detection. Anal Chem 65:
587 1524–1528
588 Ohtani K (1971) Studies on the change of hydrographic conditions in the Funka Bay. II.
589 Characteristics of the water occupying the Funka Bay. Bull Fac Fish Hokkaido Univ
590 22: 58–66 (in Japanese with English abstract)
591 Ohtani K, Akiba Y (1970) Studies on the change of hydrographic conditions in the
592 Funka Bay. I. The annual change of the water of the bay. Bull Fac Fish Hokkaido
593 Univ 20: 303–312 (in Japanese with English abstract)
594 Ohtani K, Kido K (1980) Oceanographic structure in Funka Bay. Bull Fac Fish
595 Hokkaido Univ 31: 84–114 (in Japanese with English abstract)
596 Parsons, T. R., Y. Maita and C. M Lalli (1984): A Manual of Chemical and Biological
597 Methods for Seawater Analysis. Pergamon Press, New York, 173 pp.
598 Saitoh Y, Kuma K, Isoda Y, Kuroda H, Matsuura H, Wagawa T, Takata T, Kobayashi
599 N, Nagao S, Nakatsuka T (2008) Processes influencing iron distribution in the
600 coastal waters of the Tsugaru Strait, Japan. J Oceanogr 64: 815–830
601 Sasaki K, Noriki S, Tsunogai S (2001) Vertical distributions of interstitial phosphate
602 and fluoride in anoxic sediment: Insight into the formation of an authigenic

603 fluoro-phosphorus compound. Geochem J 35: 295–306
604 Severmann S, McManus J, Berelson WM, Hammond DE (2010) The continental shelf
605 benthic iron flux and its isotope composition. Geochim Cosmochim Acta 74:
606 3984–4004
607 Shinada A, Shiga N, Ban S (1999) Structure and magnitude of diatom spring bloom in
608 Funka Bay, southwestern Hokkaido, Japan, as influenced by the intrusion of coastal
609 Oyashio water. Plank Biol Ecol 46: 24–29
610 Stigliani WM (1988) Changes in valued capacities of soils and sediments as indicators
611 of nonlinear and time-delayed environmental effects. Environmental Monitoring
612 and Assessment 10: 245–307
613 Takahashi D, Nishida Y, Kido K, Nishina K, Miyake H (2005) Formation of the
614 summertime anticyclonic eddy in Funka Bay, Hokkaido, Japan. Cont Shelf Res 25:
615 1877–1893
616 Tanaka K, Kuma K, Hamasaki K, Yamashita Y (2014) Accumulation of humic-like
617 fluorescent dissolved organic matter in the Japan Sea. Sci Rep 4: 5292,
618 doi:10.1038/srep05292
619 Uchida R, Kuma K, Omata A, Ishikawa S, Hioki N, Ueno H, Isoda Y, Sakaoka K,
620 Kamei Y, Takagi S (2013) Water column iron dynamics in the subarctic North
621 Pacific and Bering Sea. J Geophys Res 118: 1257–1271,
622 doi:10.1029/2012JC008440
623 Watanabe Y, Tsunogai S (1984) Adsorption-desorption control of phosphate in anoxic
624 sediment of a coastal sea, Funka Bay, Japan. Mar Chem 15: 71–83
625 Yoshikawa C, Nakatsuka T, Wakatsuchi M (2006) Distribution of N* in the Sea of
626 Okhotsk and its use as a biogeochemical tracer of the Okhotsk Sea Intermediate
627 Water formation process. J Mar Sys 63: 49–62
628 Yoshimura T, Kudo I (2011) Seasonal phosphorus depletion and microbial responses to
629 the change in phosphorus availability in a subarctic coastal environment. Mar Chem

126: 182–192

Figure captions

**Fig. 1** Map showing sampling locations (Stn 23: bottom depth 95 m; Stn 30: bottom depth 92 m; Stn 33: bottom depth 96 m) closely located in the center of the bay basin, in Funka Bay (Hokkaido, Japan)

**Fig. 2** Vertical distributions of temperature, salinity, and density at Stn 30 in Funka Bay during 13 August 2010–11 February 2011 (**a**–**c**) and during 13 April–14 December 2011 (**d**–**f**).

**Fig. 3** Temperature–salinity diagram at Stn 30 in Funka Bay during 13 August 2010–11 February 2011 (**a**, **c**) and during 13 April–14 December 2011 (**b**, **d**). (**c**) and (**d**) are enlargements of the areas shown in *light brown* in (**a**) and (**b**), respectively. {*Tw* Tsugaru Warm Current, *O* Oyashio Coastal Branch, *Oi* ice melting water of the Oyashio, *Fw* Funka Bay water formed in winter, *Fs* Funka Bay water formed in summer (Ohtani 1971)} Red arrow signs indicate the temporally strong intrusion of Tsugaru Warm Current into deep–bottom waters on 18 August 2011.

**Fig. 4** Vertical distributions of humic F-intensity (**a, f**) and nutrients (**b–d, g–i**) and dissolved oxygen (DO, **e, j**) concentrations at Stn 30 during 13 August 2010–11 February 2011 (**a–e**) and during 13 April–14 December 2011 (**f–j**). Light brown area shows low DO concentration below 2 ml $L^{-1}$ (**e, j**)

**Fig. 5** Seasonal variations of dissolved oxygen (DO) concentrations, which were

measured at 90 m depth of Stn 30 during April–October in 2010 and 2011 by a DO sensor. Light brown area shows low DO concentration below 2 ml $L^{-1}$.

**Fig. 6** Vertical distributions of dissolved iron (D-Fe, **a–d**) and total dissolvable iron (T-Fe, **e–h**) concentrations at Stn 23, Stn 33, and Stn 30 during 13 August 2010–11 February 2011 (**a–c, e–g**) and at Stn 30 during 13 April–14 December 2011 (**d, h**).

**Fig. 7** Humic F-intensity versus salinity in deep–bottom waters (≥70 m) at Stn 23, Stn 33, and Stn 30. (*TW* Tsugaru Warm water, *OW* Oyashio water)

**Fig. 8** $PO_4$ (**a**) and $Si(OH)_4$ (**b**) versus AOU in deep–bottom waters (≥70 m) at Stn 23, Stn 33, and Stn 30.

**Fig. 9** $NO_3 + NO_2$ versus AOU (**a**) and $NO_3 + NO_2$ versus $PO_4$ (**b**) in deep–bottom waters (≥70 m) at Stn 23, Stn 33, and Stn 30.

**Fig. 10** D-Fe versus AOU in deep–bottom waters (≥70 m) at Stn 23, Stn 33, and Stn 30. Each curve was obtained by power fitting of the data in August and October 2010, in December 2010, and in August and October 2011.

Fig. 1 Hioki et al.

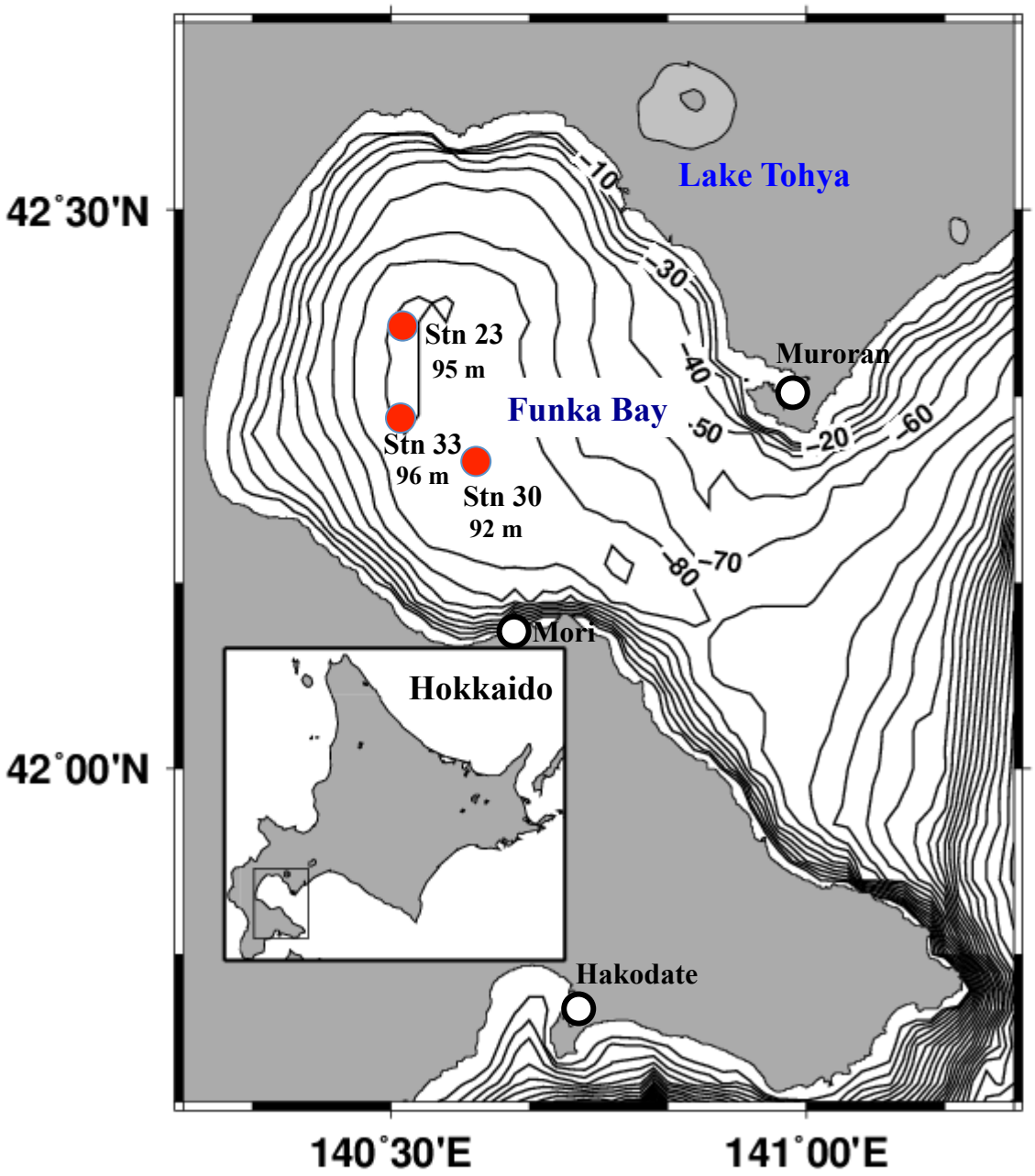

Fig. 2 Hioki et al.

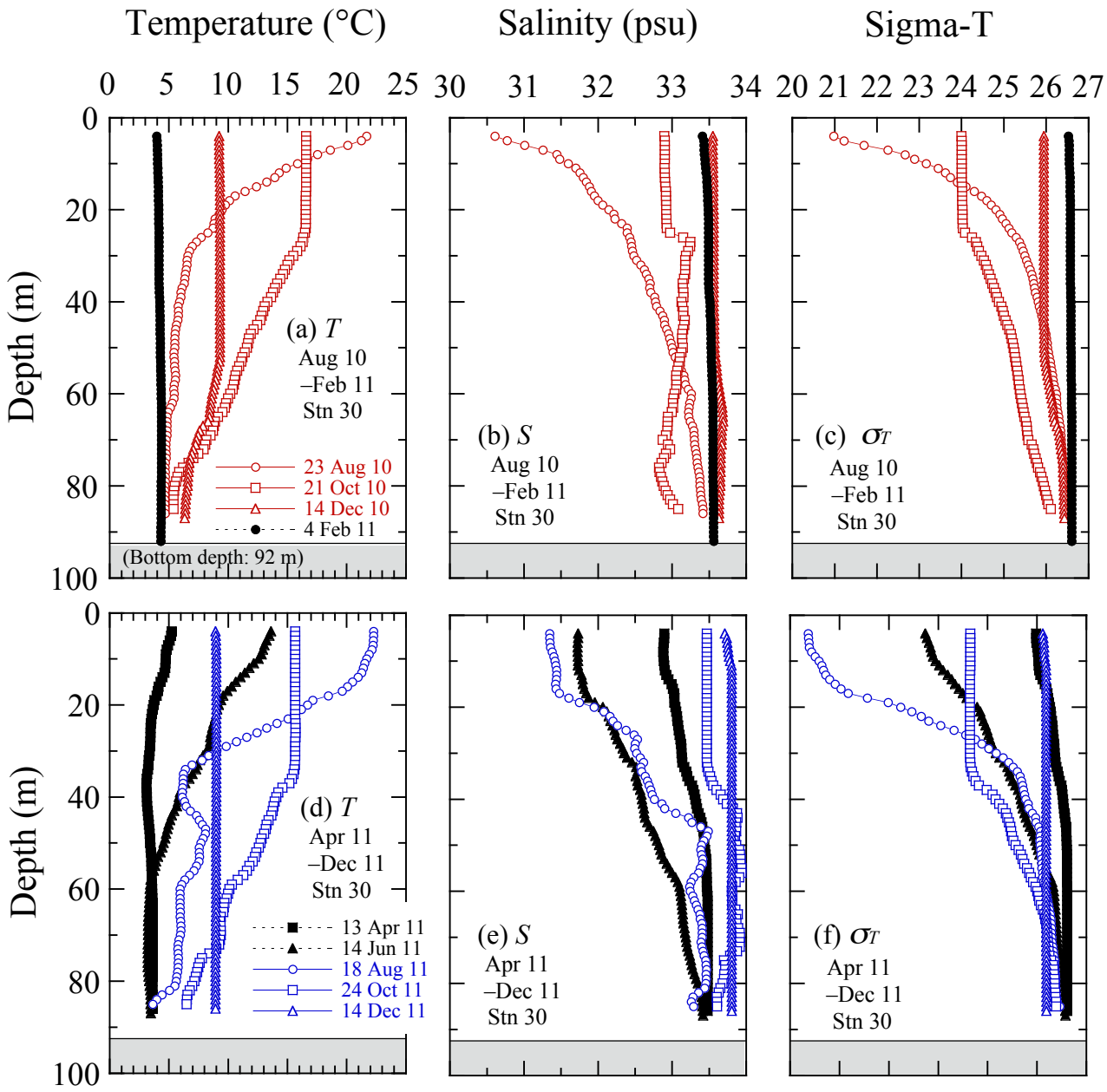

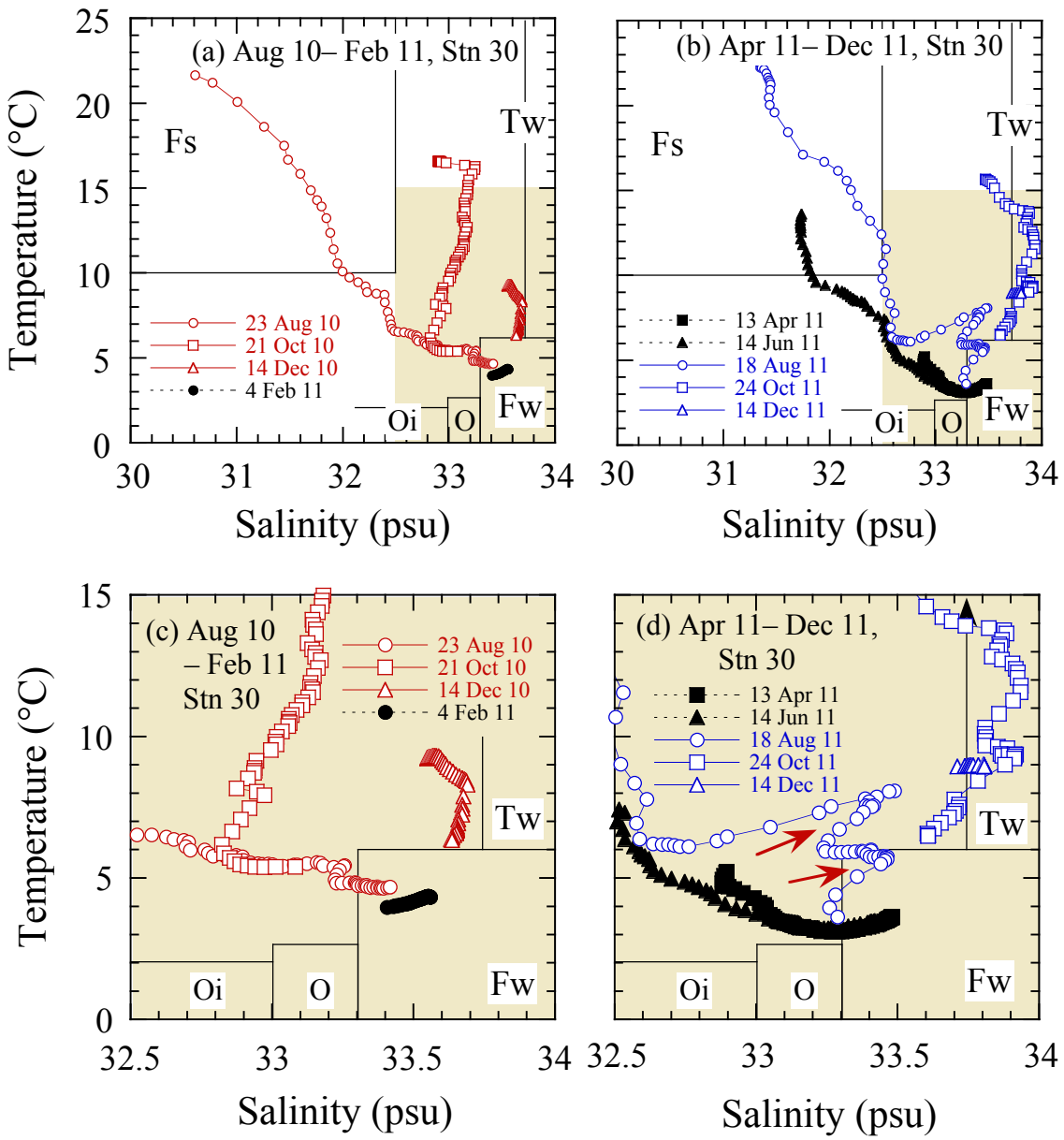
(a) Aug 10– Feb 11, Stn 30
(b) Apr 11– Dec 11, Stn 30
(c) Aug 10 – Feb 11 Stn 30
(d) Apr 11– Dec 11, Stn 30
Temperature (°C)
Salinity (psu)
Fs
Tw
Oi
O
Fw
23 Aug 10
21 Oct 10
14 Dec 10
4 Feb 11
13 Apr 11
14 Jun 11
18 Aug 11
24 Oct 11
14 Dec 11

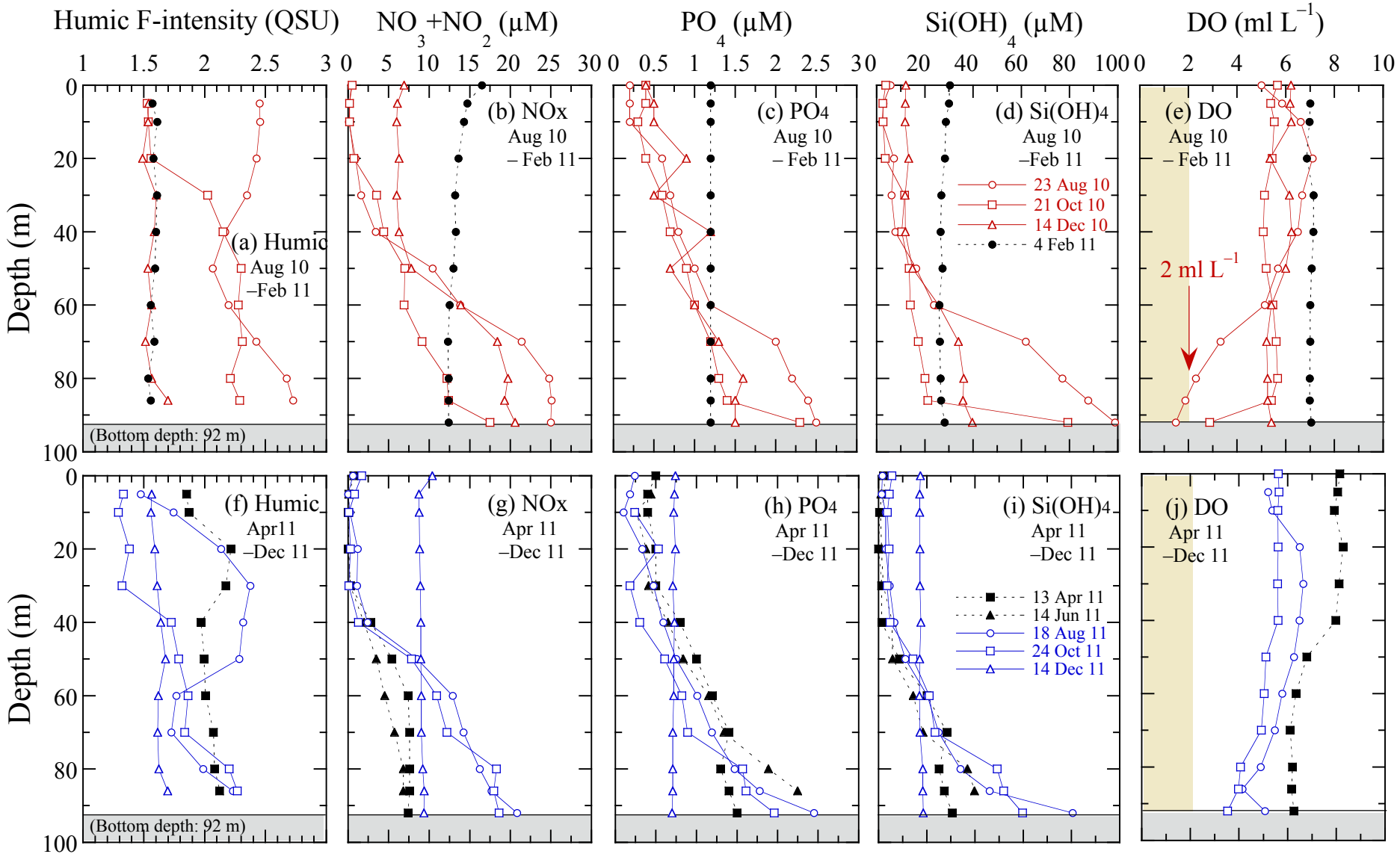
Humic F-intensity (QSU)
NO3+NO2 (μM)
PO4 (μM)
Si(OH)4 (μM)
DO (ml L−1)
Depth (m)
(a) Humic
Aug 10
–Feb 11
(b) NOx
Aug 10
– Feb 11
(c) PO4
Aug 10
– Feb 11
(d) Si(OH)4
Aug 10
–Feb 11
23 Aug 10
21 Oct 10
14 Dec 10
4 Feb 11
(e) DO
Aug 10
– Feb 11
2 ml L−1
(Bottom depth: 92 m)
(f) Humic
Apr11
–Dec 11
(g) NOx
Apr 11
–Dec 11
(h) PO4
Apr 11
–Dec 11
(i) Si(OH)4
Apr 11
–Dec 11
13 Apr 11
14 Jun 11
18 Aug 11
24 Oct 11
14 Dec 11
(j) DO
Apr 11
–Dec 11
(Bottom depth: 92 m)

Fig. 5 Hioki et al.

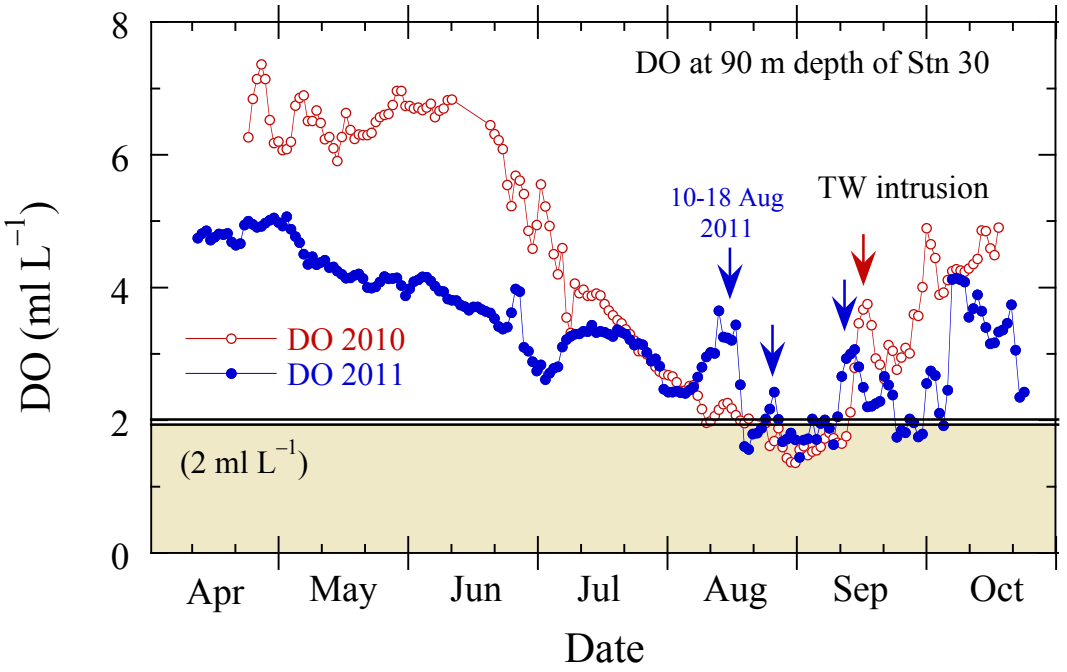

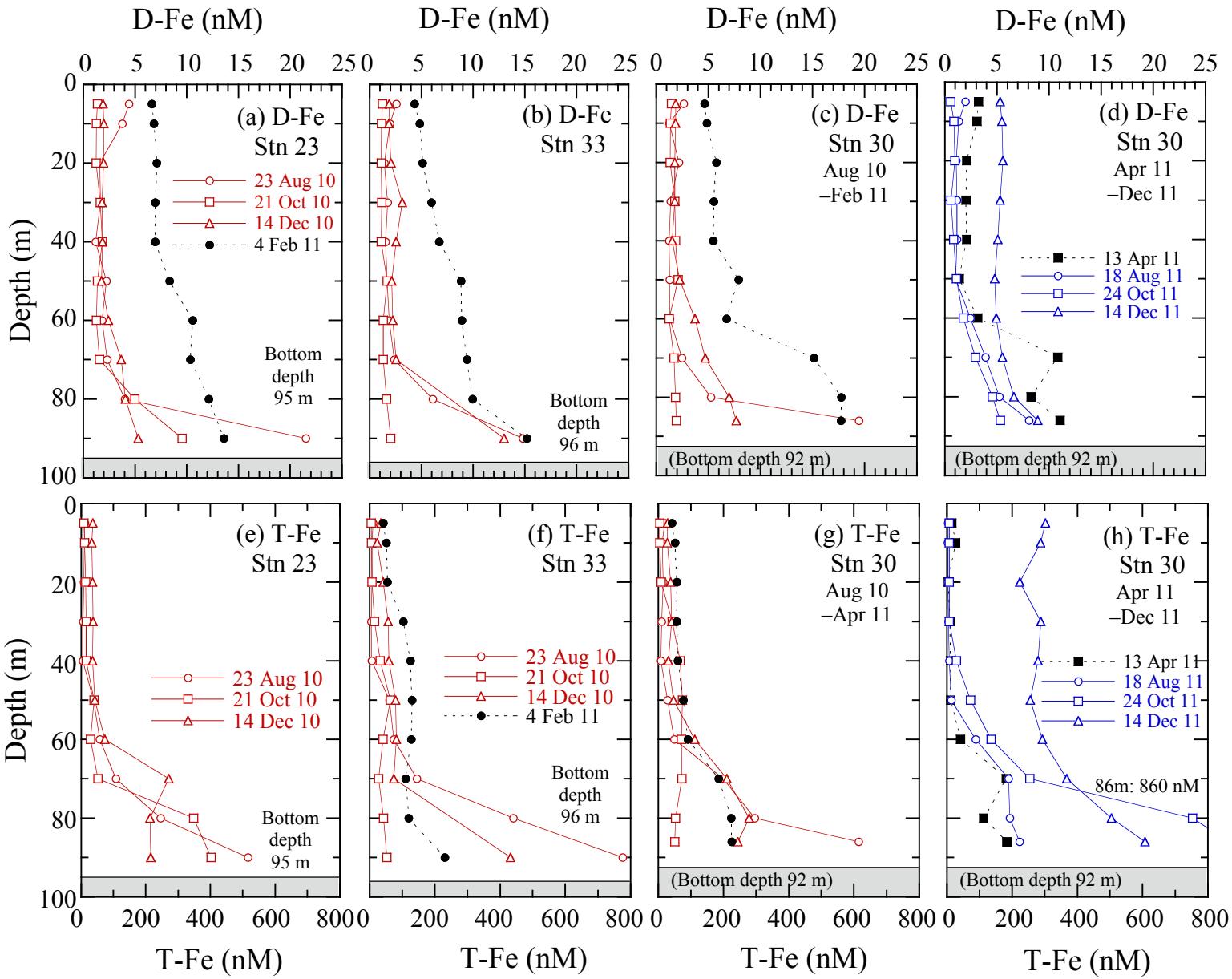
D-Fe (nM)
T-Fe (nM)
Depth (m)
(a) D-Fe
Stn 23
23 Aug 10
21 Oct 10
14 Dec 10
4 Feb 11
Bottom
depth
95 m
(b) D-Fe
Stn 33
Bottom
depth
96 m
(c) D-Fe
Stn 30
Aug 10
–Feb 11
(Bottom depth 92 m)
(d) D-Fe
Stn 30
Apr 11
–Dec 11
13 Apr 11
18 Aug 11
24 Oct 11
14 Dec 11
(Bottom depth 92 m)
(e) T-Fe
Stn 23
(f) T-Fe
Stn 33
(g) T-Fe
Stn 30
Aug 10
–Apr 11
(h) T-Fe
Stn 30
Apr 11
–Dec 11
86m: 860 nM

Fig. 7 Hioki et al.

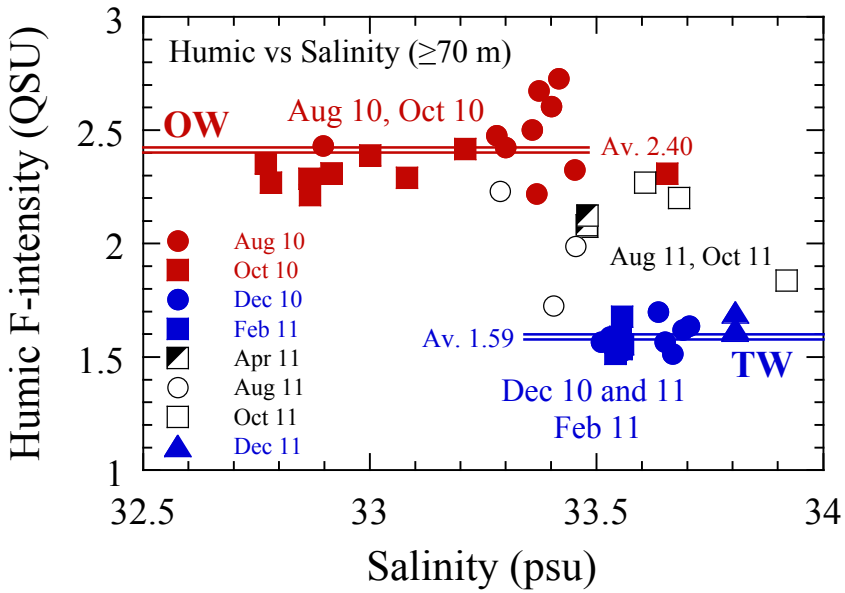

Fig. 8 Hioki et al.

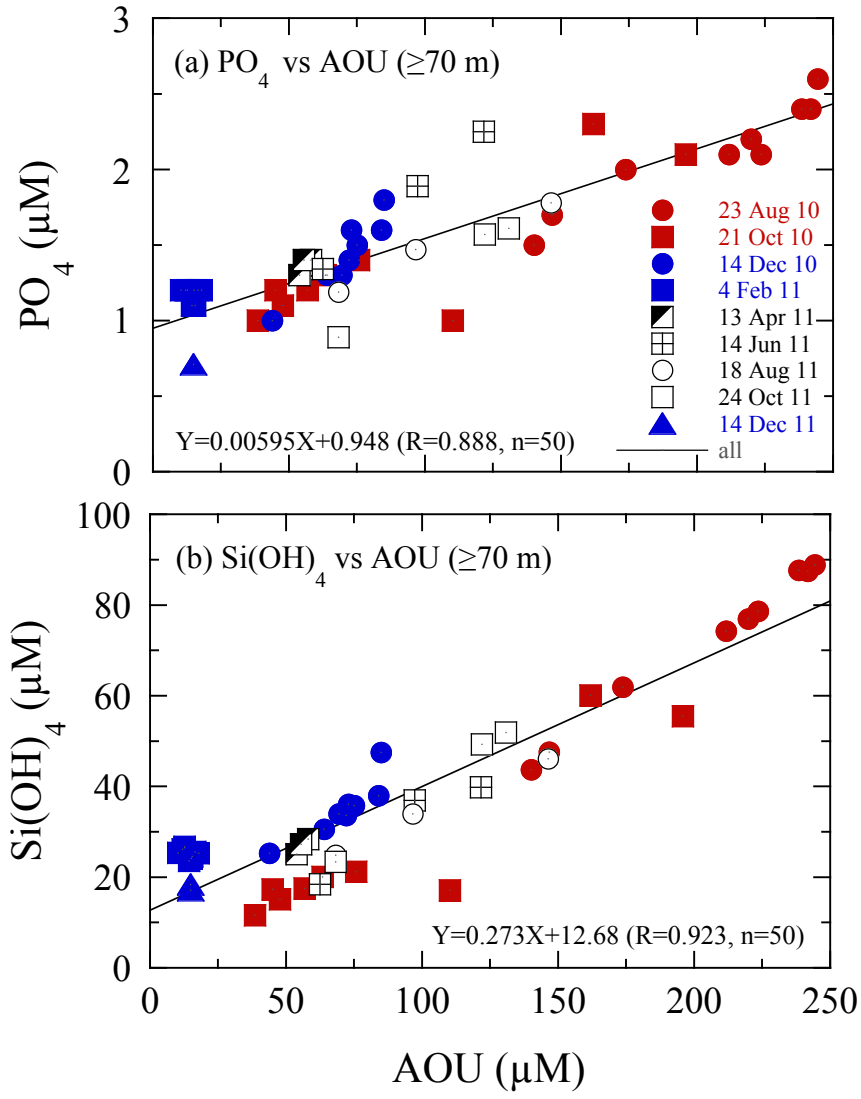

Fig. 9 Hioki et al.

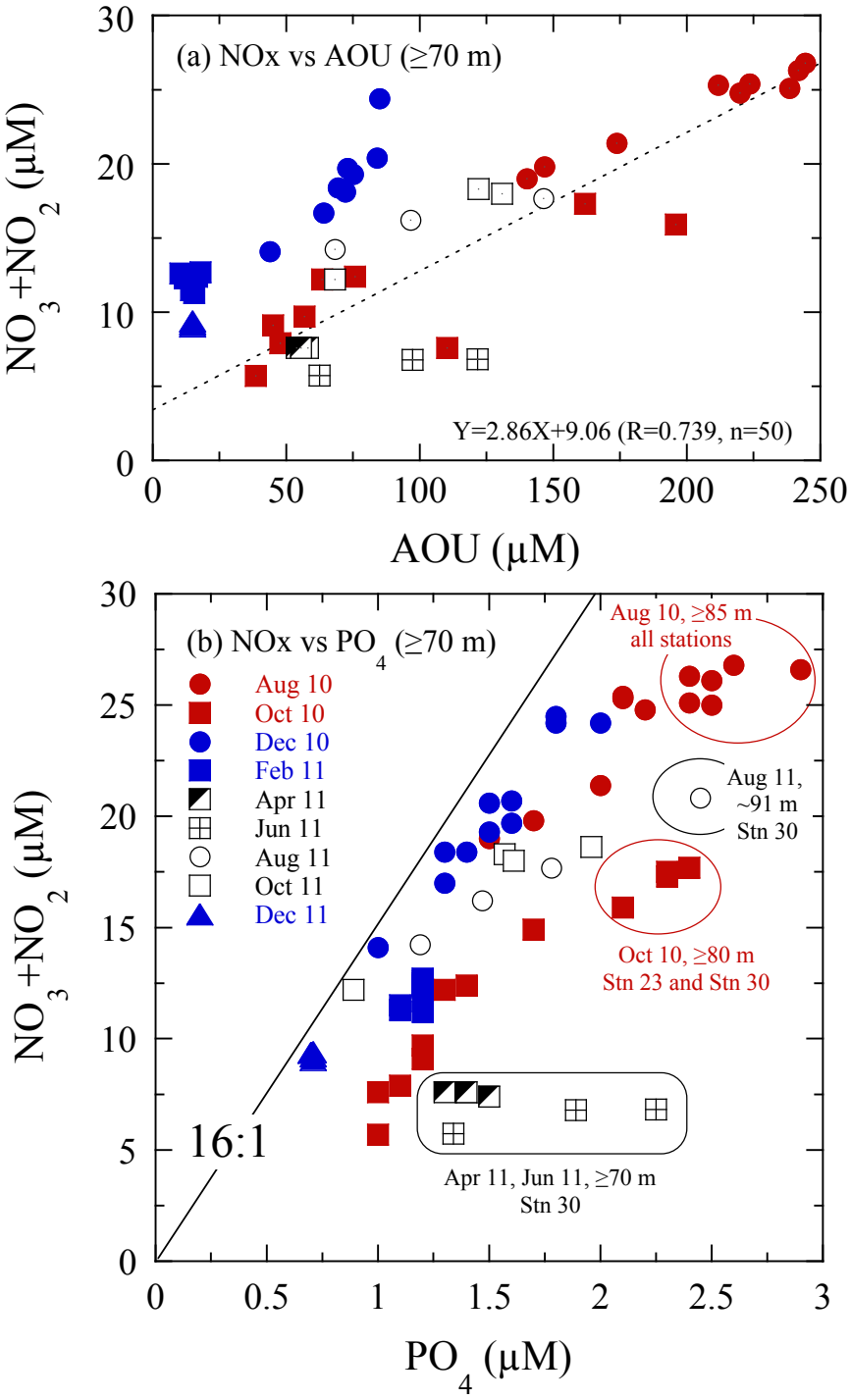

Fig. 10 Hioki et al.